ACS Sustainable Chemistry & Engineering

Research Article

Cite This: ACS Sustainable Chem. Eng. 2019, 7, 9017−9027

pubs.acs.org/journal/ascecg

Development of a Thermophysical Properties Model for Flowsheet Simulation of Biomass Pyrolysis Processes

Maximilian B. Gorensek,*[,†] Rajasi Shukre,[‡] and Chau-Chyun Chen[‡]

[†]Secure Energy Manufacturing, Savannah River National Laboratory, Savannah River Site, 703-41A/225, Aiken, South Carolina 29808, United States

[‡]Department of Chemical Engineering, Texas Tech University, P.O. Box 43121, Lubbock, Texas 79409-3121, United States

Supporting Information

ABSTRACT: A properties model was developed for use in commercial process simulators to model pyrolysis of lignocellulosic biomass. The component list was chosen to enable process simulations based on a recently published lumped pyrolysis kinetics model. Since many of the compounds involved in pyrolysis are not found in simulator databanks, estimation based on available literature data was used to establish missing parameters. Standard solid enthalpy of formation, solid heat capacity, and solid density estimates calculated from the limited experimental data available were prepared for six biomass constituents and nine intermediate and end-products of their pyrolysis. Ideal gas enthalpy of formation and heat capacity, critical property, and vapor pressure estimates were prepared for another four pyrolysis end-products and one biomass component. The estimates were all validated against the closest available experimental data in the literature. The addition of these new components and properties allows thermodynamically rigorous simulation of lumped biomass pyrolysis reactions with accurate energy balances. Enthalpies of reaction calculated from the properties model were compared with reported reaction enthalpies for the same lumped biomass pyrolysis reactions and found to be in general agreement.

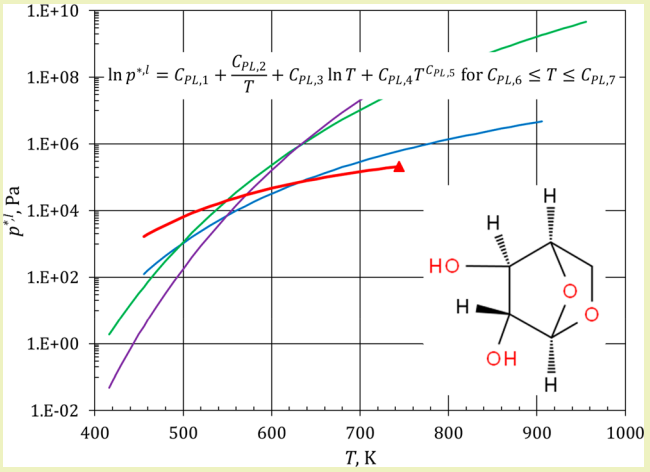

KEYWORDS: *Biomass pyrolysis, Thermophysical property parameters, Property estimation, Pyrolysis reaction enthalpy, Pyrolysis process flowsheet simulation*

INTRODUCTION

Thermophysical property model parameters for many of the components involved in biomass pyrolysis are missing from the pure component databanks of commercial process simulators. This is due to the complexity of biomass and the practice of relying on hypothetical "model compounds" which cannot be isolated for measurement of their thermophysical properties.[1−4] Since the fidelity of a process model hinges on the fidelity of its underlying properties model, care must be taken to ensure that the parameter estimation methods used yield model parameters that result in credible property estimates. For example, the energy balance for a pyrolysis reactor model demands accurate evaluation of the enthalpies of formation for all species participating in the various pyrolysis reactions. The estimation of missing property parameters for biomass process models has been addressed previously by others.[5,6] This paper presents a complete properties model for biomass pyrolysis processes developed for aspenONE (but applicable to other modeling platforms, such as ChemCAD, gPROMS, and Pro/II Process Engineering) with carefully screened properties estimates.

The three principal building blocks of lignocellulosic biomass are cellulose, hemicellulose, and lignin. Other important components include extractives, moisture, and ash. Pyrolysis process models treat these as chemical species with a defined molecular formula and thermophysical properties that need to be in atom, material, and energy balance with the reaction products and process energy inputs and outputs.[1−4] For this work, the pyrolytic decomposition mechanism of Ranzi et al.[1] was chosen as the baseline and consequently determines the additional chemical species for which property models and parameters must be provided.

Ranzi et al. assume that biomass is made up of 10 distinct components: cellulose, two types of hemicellulose (gluco-mannan/softwood and xylan/hardwood), three types of lignin (carbon-, hydrogen-, and oxygen-rich), two extractives (tannin and triglyceride), moisture, and ash.[1] Of these, only the last two have relevant pure component property parameters in the

Received: March 4, 2019
Revised: March 28, 2019
Published: April 5, 2019

DOI: 10.1021/acssuschemeng.9b01278
ACS Sustainable Chem. Eng. 2019, 7, 9017−9027

Table 1. Chemical Species Used in the Biomass Pyrolysis Process Model

chemical compound	component ID	type	component name	formula
		Biomass Components		
tannin	TANN	solid		$C_{15}H_{12}O_7$
C-rich lignin	LIGC	solid		$C_{15}H_{14}O_4$
O-rich lignin	LIGO	solid		$C_{20}H_{22}O_{10}$
H-rich lignin	LIGH	solid		$C_{22}H_{28}O_9$
triglyceride	TGL	conventional		$C_{57}H_{100}O_7$
hemicellulose-glucomannan	GMSW	solid		$C_5H_8O_4$
hemicellulose-xylan	XYHW	solid		$C_5H_8O_4$
cellulose	CELL	solid		$C_6H_{10}O_5$
ash	ASH	solid	CALCIUM-OXIDE	CaO
moisture	H2OL	conventional	WATER	H_2O
		Biomass Pyrolysis Intermediate Species		
secondary lignin intermediate	LIG	solid		$C_{11}H_{12}O_4$
C-rich lignin intermediate	LIGCC	solid		$C_{15}H_{14}O_4$
H/O-rich lignin intermediate	LIGOH	solid		$C_{19}H_{22}O_8$
activated hemicellulose 1	HCE1	solid		$C_5H_8O_4$
activated hemicellulose 2	HCE2	solid		$C_5H_8O_4$
activated cellulose	CELLA	solid		$C_6H_{10}O_5$
tannin intermediate	ITANN	solid		$C_8H_4O_4$
		Biomass Pyrolysis End-Products		
char	CHAR	solid	CARBON-GRAPHITE	C
sinapyl aldehyde	FE2MACR	conventional		$C_{11}H_{12}O_4$
free fatty acid	FFA	conventional	LINOLEIC-ACID	$C_{18}H_{32}O_2$
high-molecular-weight lignin	HMWL	solid		$C_{24}H_{28}O_4$
glyoxal	GLYOX	conventional	GLYOXAL	$C_2H_2O_2$
ethylene	C2H4	conventional	ETHYLENE	C_2H_4
acetaldehyde	CH3CHO	conventional	ACETALDEHYDE	C_2H_4O
acetic acid	ACAC	conventional	ACETIC-ACID	$C_2H_4O_2$
glycol aldehyde	HAA	conventional	GLYCOL-ALDEHYDE	$C_2H_4O_2$
ethanol	C2H5OH	conventional	ETHANOL	C_2H_6O
acrolein	ACROL	conventional	ACROLEIN	C_3H_4O
n-propionaldehyde	ALD3	conventional	N-PROPIONALDEHYDE	C_3H_6O
3-hydroxypropanal	C3H6O2	conventional		$C_3H_6O_2$
furfural	FURF	conventional	FURFURAL	$C_5H_4O_2$
xylosan	XYLAN	conventional		$C_5H_8O_4$
levoglucosan	LVG	conventional	LEVOGLUCOSAN	$C_6H_{10}O_5$
phenol	PHENOL	conventional	PHENOL	C_6H_6O
5-hydroxymethyl-furfural	HMFU	conventional	5-HYDROXY-METHYLFURFURAL	$C_6H_6O_3$
anisole	ANISOLE	conventional	METHYL-PHENYL-ETHER	C_7H_8O
p-coumaryl alcohol	COUMARYL	conventional		$C_9H_{10}O_2$
formaldehyde	CH2O	conventional	FORMALDEHYDE	CH_2O
formic acid	HCOOH	conventional	FORMIC-ACID	CH_2O_2
methane	CH4	conventional	METHANE	CH_4
methanol	CH3OH	conventional	METHANOL	CH_4O
carbon monoxide	CO	conventional	CARBON-MONOXIDE	CO
carbon dioxide	CO2	conventional	CARBON-DIOXIDE	CO_2
hydrogen	H2	conventional	HYDROGEN	H_2
water	H2O	conventional	WATER	H_2O
		Nonbiomass Components		
argon	AR	conventional	ARGON	Ar
nitrogen	N2	conventional	NITROGEN	N_2
oxygen	O2	conventional	OXYGEN	O_2
sand	SAND	solid	SILICON-DIOXIDE	SiO_2

aspenONE databanks. Thus, pure component property parameters need to be estimated for 8 of the 10 biomass constituents.

Ranzi et al. also assume that each biomass constituent behaves independently under pyrolysis. Seven form reactive intermediates that undergo further decomposition. The intermediates include activated cellulose, two activated hemicelluloses, three lignin intermediates, and a tannin intermediate.[1] None of these are in the aspenONE pure component databanks, so property parameter estimation is needed for them as well.

Finally, Ranzi et al.'s mechanism has 28 end-products, five of which are not found in the databanks. All told, then, pure

DOI: 10.1021/acssuschemeng.9b01278
ACS Sustainable Chem. Eng. 2019, 7, 9017−9027

component parameters need to be estimated for 20 species to be able to model a fast pyrolysis process using this mechanism.

MODEL COMPONENTS

The 49 species which comprise the biomass fast pyrolysis process properties model are listed in Table 1. Component IDs used in the process model are shown in column two. The third column indicates whether the species is treated as a "conventional" (fluid) component that participates in vapor−liquid equilibrium (VLE) or as a (conventional) "solid" that is inert with respect to VLE. Component names used by the aspenONE databanks are listed in the fourth column for those species that are included in the databanks. An empty space indicates that the databanks do not have any entries for that species. The last column provides the chemical formulas, which, for the polymeric holocellulose and lignin species, are those of the monomer building blocks. (All molar properties of the polymeric species are per monomer unit.)

Table 1 is subdivided into four groupings. The first 10 species are the constituents of unpyrolyzed biomass. Eight are treated as conventional solids. No databank entries exist for the first eight. The moisture content of water is tracked separately from water vapor, although its properties are the same. Ash content is treated as calcium oxide for which pure component property parameters are available. The next grouping lists the seven intermediate products of biomass pyrolysis. None of these appear in the databanks, and all are treated as conventional solids. The third grouping is the largest and includes the 28 end-products of pyrolysis. All but two (char and high-molecular-weight lignin) are treated as conventional fluid components. Five (sinapyl aldehyde, high-molecular-weight lignin, 3-hydroxypropanal, xylosan, and *p*-coumaryl alcohol) are not included in the databanks. The last grouping in Table 1 is the four nonbiomass constituents of dry air and (silica) sand. All appear in the databanks. The gaseous elements are treated as conventional fluids, while sand is a conventional solid.

THERMODYNAMIC FRAMEWORK

The Peng−Robinson cubic equation of state with Boston−Mathias alpha function[7] was chosen as the thermodynamic basis for calculating the properties of biomass pyrolysis process streams. Suitable for simulation of nonpolar or mildly polar mixtures of hydrocarbons and light gases, it is known as the PR-BM method in Aspen Plus[8] and is recommended for gas-processing, refinery, and petrochemical applications. PR-BM has been the properties method of choice by others to model biomass pyrolysis processes.[2−4]

To use the PR-BM method, all solid components must have values for molecular weight and the standard solid heat of formation as well as solid molar heat capacity and solid molar volume model parameters. All conventional fluid components must have values for molecular weight, ideal gas standard state heat of formation, critical temperature, critical pressure, and acentric factor as well as vapor pressure and ideal gas molar heat capacity parameters.

Conventional Solid Component Parameter Estimates. Property parameter values for the 15 conventional solid compounds will be addressed first.

Standard Solid Heat of Formation. The standard heat of formation of a solid compound can be estimated if experimental data are available for the heat of combustion of that compound.[9] In the event such data are lacking, the heat of combustion per unit mass of any member of a class of compounds can be assumed to be the same, so that the molar heat of combustion for an individual member of the same class can be estimated, as a first approximation, by multiplying the mass-based value for any other member by its molecular weight.

The 15 conventional solids include seven lignin species. Experimental heats of combustion were recently reported for lignin extracted from rape straw by two different methods.[10] The lignin extracted using sulfuric acid, with stoichiometric composition $C_{10}H_{11.5}O_{3.9}$, is closer in oxygen content to that of the seven lignin species for which property estimates are needed and, thus, is used as the reference species here. Tannins are complex polyphenolic compounds that share aromaticity and oxygenation with lignin. In the absence of any heat of combustion data for tannins, the assumption that their heat of combustion per unit mass is similar to that of lignins seems reasonable. Thus, the experimental heat of combustion per unit mass at 298.15 K for lignin extracted from rape straw using sulfuric acid, 25.13 kJ/g,[10] was taken as the starting point for estimating the standard solid enthalpies of formation for the seven lignin and two tannin species.

The oxygen content of these nine species varies significantly. Oxygen:carbon ratios range from a high of 1:2 for LIGO and ITANN to a low of 1:6 for HMWL. More highly oxygenated compounds would be expected to have lower heats of combustion per unit mass than those with less oxygen. Consequently, adjustments need to be made to account for these differences.

Six pairs of oxygenated aromatic compounds with similar structures and chemical formulas that differ only in the number of oxygen atoms per molecule and that have experimentally determined enthalpies of combustion in the literature[11−18] were identified. Three pairs differed by one oxygen atom, while the remaining three pairs differed by two. The average difference in the standard enthalpy of combustion for each pair was 208.9 kJ/g mol/O atom (see the Supporting Information). This provides an estimate of the correction that needs to be applied to account for the differences between the oxygen content of the lignin model compounds and the lignin used in the combustion experiments.[10]

Similar adjustments can be made for differences in carbon and hydrogen number. Estimates of the individual contributions of differences in C and H atom number to the enthalpy of combustion can be made by considering the effect of CH_2, CH, and C number differences in experimental heats of combustion. For CH_2, standard enthalpies of combustion of solid alkanes with different carbon number can be exploited to show that the average contribution of the CH_2 group to the solid standard enthalpy of combustion is −651.1 kJ/g mol (see the Supporting Information).

Differences in the standard enthalpies of combustion for solid polycyclic aromatics with different carbon and hydrogen number can be used to estimate the effect of CH and C differences, e.g., naphthalene ($C_{10}H_8$, $^c\Delta H°$(naphthalene(s)) = −5156.95 kJ/g mol[19]), anthracene ($C_{14}H_{10}$, $^c\Delta H°$(anthracene(s)) = −7065 kJ/g mol[20]), and pyrene ($C_{16}H_{10}$, $^c\Delta H°$(pyrene(s)) = −7850.79 kJ/g mol[21]). Pyrene has two more carbon atoms than anthracene, and the difference in their standard enthalpies of combustion is −785.79 kJ/g mol, resulting in an estimated −392.9 kJ/g mol/C atom. Removing two carbon atoms from naphthalene would result in a hypothetical C_8H_8 compound, with a standard enthalpy of combustion of −5156.95 kJ/g mol − (−785.79 kJ/g mol) = −4371.16 kJ/g

DOI: 10.1021/acssuschemeng.9b01278
ACS Sustainable Chem. Eng. 2019, 7, 9017−9027

Table 2. Estimated Solid Property Model Parameters for Conventional Solids

component ID	molecular weight, kg/kmol	standard solid enthalpy of formation, kJ/g mol	heat capacity model coefficients		solid density, kmol/m^3
			C_1, J/(g mol K)	C_2, J/(g mol K^2)	
		Lignins and Tannins			
LIG	208.213 88	−729.31	13.2251	0.828 34	7.3002
LIGC	258.273 76	−759.39	16.4048	1.027 49	5.8852
LIGCC	258.273 76	−759.39	16.4048	1.027 49	5.8852
LIGH	436.458 92	−1722.7	27.7226	1.736 36	3.4826
LIGO	422.388 68	−1847.5	26.8289	1.680 39	3.5986
LIGOH	378.378 88	−1429.2	24.0335	1.505 30	4.0171
HMWL	380.483 92	−958.26	24.1672	1.513 68	3.9949
ITANN	164.117 36	−616.98	10.4242	0.652 91	9.2617
TANN	304.256 08	−1079.7	19.3254	1.210 42	4.9958
		Cellulose Species			
CELL	162.1424	−1019.0	−1.5328	0.675 27	9.3745
CELLA	162.1424	−1019.0	−1.5328	0.675 27	9.3745
		Hemicellulose Species			
XYHW	132.116 12	−759.2	−1.2489	0.550 22	11.5050
GMSW	132.116 12	−759.2	−1.2489	0.550 22	11.5050
HCE1	132.116 12	−759.2	−1.2489	0.550 22	11.5050
HCE2	132.116 12	−759.2	−1.2489	0.550 22	11.5050

mol. Dividing by 8, the contribution of each CH unit to the standard enthalpy of combustion can be estimated as −546.4 kJ/g mol.

Finally, given that contributions to the standard enthalpy of combustion for CH_2, CH, and C have been estimated at −651.1, −546.4, and −392.9 kJ/g mol, respectively, the difference between CH and C is −153.5 kJ/g mol, while that between CH_2 and C is −104.7 kJ/g mol, for an average difference of −129.1 kJ/g mol/H atom. The corrections that can be applied to the standard enthalpy of combustion of sulfuric lignin, therefore, are 208.9 kJ/g mol/O atom, −392.9 kJ/g mol/C atom, and −129.1 kJ/g mol/H atom.

The standard enthalpies of formation for the lignins and tannins can now be calculated, as shown below for LIGO. The monomeric formula for LIGO is $C_{20}H_{22}O_{10}$, while that reported for sulfuric lignin is $C_{10}H_{11.5}O_{3.9}$. To minimize differences in C, H, and O numbers, the calculation considers the dimer formula for sulfuric lignin instead, $C_{20}H_{23}O_{7.8}$, which, given a measured standard enthalpy of combustion of −25.13 kJ/g,[10] results in a molar value of −9755.4 kJ/g mol. The LIGO monomer has the same carbon number but 1 fewer hydrogen atom and 2.2 more oxygen atoms than the sulfuric lignin dimer. Corrections of (0 C atom) × (−392.9 kJ/g mol/C atom) + (−1 H atom) × (−129.1 kJ/g mol/H atom) + (+2.2 O atom) × (208.9 kJ/g mol/O atom) result in an estimated standard enthalpy of combustion for LIGO equal to −9166.8 kJ/g mol LIGO. The combustion of LIGO can be represented by the following reaction:

$$C_{20}H_{22}O_{10}10(s) + 20\frac{1}{2}O_2(g) \Rightarrow 20CO_2(g) + 11H_2O(l)$$

$$^{c}\Delta H^{\circ}(\mathrm{LIGO(s)}) = -9166.8\ \mathrm{kJ/g\ mol}$$

Thus, the standard enthalpy of formation for LIGO can now be calculated from the standard enthalpy of combustion and the standard enthalpies of formation for $CO_2(g)$ and $H_2O(l)$:[22]

$$^{f}\Delta H^{\circ}(\mathrm{LIGO(s)}) = -{}^{c}\Delta H^{\circ}(\mathrm{LIGO(s)}) + 20\,{}^{f}\Delta H^{\circ}(\mathrm{CO2(g)}) + 11\,{}^{f}\Delta H^{\circ}(\mathrm{H2O(l)}) = -1847.5\ \mathrm{kJ/g\ mol}$$

Standard enthalpies of formation estimated in this manner for the nine lignins and tannins are listed in the third column of the first grouping in Table 2. Dimeric sulfuric lignin was used as the basis for LIGO, LIGH, LIGOH, HMWL, and TANN, while the monomeric form was the starting point for the others. The heating value of biomass is well correlated with proximate and ultimate analyses,[23] providing a way to validate these results. A comparison of the estimated standard enthalpies of combustion for the nine lignins and tannins with higher heating values calculated from their ultimate analyses using the correlation developed by Channiwala and Parikh[24] shows good agreement. The estimates exhibit an average deviation of −1.5% and a maximum deviation of −2.1% from the correlation, confirming the validity of this approach (see the Supporting Information).

Estimating the standard enthalpy of formation for the holocellulosic solids was much more straightforward. Experimental heats of combustion have also been recently reported for cellulose extracted from four different sources in four differing ways.[25] The mean value for all four samples was −2771.25 kJ/g mol, based on $C_6H_{10}O_5$ as the monomer. Following the same procedure as for the lignins, this results in a standard enthalpy of formation of −1019.0 kJ/g mol. Activated cellulose is chemically identical to cellulose, so its standard enthalpy of formation is assumed to be the same as that of cellulose. Standard enthalpies of formation for the two cellulosic species are listed in the third column of the second grouping in Table 2.

Heat of combustion data for hemicellulose have proven harder to find. A recent paper reports the results of higher heating value measurements for a variety of biopolymers including birch wood xylan.[26] The value measured for xylan, −17.80 kJ/g, can be used to estimate the heat of formation for hemicellulose in a manner similar to that for the lignins. Although the Ranzi et al. pyrolysis reaction mechanism distinguishes between hardwood (xylan) and softwood (glucomannan) hemicelluloses, both are shown as having the same monomer formula, $C_5H_8O_4$, which is that of xylan and different from glucomannan ($C_{24}H_{42}O_{21}$). Consequently, the heat of formation estimated from the higher heating value of xylan is used for both hardwood and softwood hemicellulose as

DOI: 10.1021/acssuschemeng.9b01278
ACS Sustainable Chem. Eng. 2019, 7, 9017−9027

Table 3. Estimated Fluid Property Model Parameters for Conventional Fluids

	3-hydroxypropanal	triglyceride	*p*-coumaryl alcohol	sinapyl aldehyde	xylosan
molecular weight, kg/kmol	74.079 44	897.4168	150.1772	208.213 88	132.116 12
ideal gas enthalpy of formation, kJ/g mol	−345.3	−1546.3	−193.5	−483.8	−642.3
critical temperature, K	605.0	934.6	791.4	837.9	744.3
critical pressure, bar	56.36	2.027	56.90	29.25	2.134
acentric factor	1.133	2.084 19	1.198	0.981	0.292
Ideal Gas Heat Capacity Estimates, J/g mol-K					
$C_P^{*,ig}$(298 K)	91.46	1304.35	177.30	240.85	142.76
$C_P^{*,ig}$(400 K)	109.33	1648.81	225.11	302.37	179.06
$C_P^{*,ig}$(500 K)	126.37	1950.68	264.73	357.37	215.39
$C_P^{*,ig}$(600 K)	141.02	2194.89	296.16	402.54	240.55
$C_P^{*,ig}$(800 K)	164.75	2564.01	342.81	471.36	281.03
$C_P^{*,ig}$(1000 K)	182.00	2840.98	374.75	520.31	307.48
Aly−Lee $C_P^{*,ig}$ Equation Coefficients					
$C_{CP,1}$, J/(kmol K)	77 793.84	1 008 344	128 972.6	190 226.6	115 298.4
$C_{CP,2}$, J/(kmol K)	106 997.7	1 979 396	342 667.4	491 979.1	224 458.5
$C_{CP,3}$, K	814.165	777.2196	1575.222	1728.691	824.2086
$C_{CP,4}$, J/(kmol K)	66 750.56	1 165 050	266 861.9	371 592.6	59 411.96
$C_{CP,5}$, K	2048.402	2438.886	728.2816	797.2112	2302.592
$C_{CP,6}$, K	298	298.15	298	298	298
$C_{CP,7}$, K	1000	1500	1000	1000	1000
Extended Antoine Equation Coefficients, K/Pa:					
$C_{PL,1}$	136.9781	234.71	286.7075	286.6149	135.2637
$C_{PL,2}$	−13 924.84	−34 699	−25 124.63	−25 391.53	−14 336.53
$C_{PL,3}$	−15.464 95	−27.25	−37.267 39	−37.287 66	−15.745 01
$C_{PL,4}$	$1.303\,768 \times 10^{-17}$	1.5475×10^{-18}	$1.486\,27 \times 10^{-5}$	$1.361\,18 \times 10^{-5}$	$2.245\,921 \times 10^{-18}$
$C_{PL,5}$	6	6	2	2	6
$C_{PL,6}$	261.15	262.15	406.15	406.15	455.4
$C_{PL,7}$	605	934.6	791.4	837.9	744.3

well as their two activated forms (third column of the third grouping in Table 2).

Solid Heat Capacity Polynomial. As was the case for the heat of combustion, the heat capacity per unit mass of any member of a class of compounds can be assumed to be the same, so that the molar heat capacity for an individual member of that class can be approximated by multiplying the mass-based value for any other member by its molecular weight. The same source that reported experimental heats of combustion for rape straw also measured heat capacities.[10] Experimentally measured values of the solid mass heat capacity of lignin extracted using sulfuric acid, with stoichiometric composition $C_{10}H_{11.5}O_{3.9}$, were provided over the temperature range from 79.4 to 368.5 K. These were fitted to a linear equation by least-squares regression, assumed to be applicable to any of the lignins or tannins, and converted to molar basis by multiplying by the appropriate molecular weight (see the Supporting Information). Values of the first two coefficients of the solid molar heat capacity polynomial estimated in this way for the nine lignins and tannins are listed in the fourth and fifth columns of the first grouping in Table 2 (quadratic and higher-order coefficients should be set to zero).

Experimental measurements of the solid heat capacity of cellulose are reported in the same source that provided heat of combustion data.[25] A linear model was fitted to all the data above 80 K and converted to a molar basis by multiplication by the molecular weight of cellulose (see the Supporting Information). It is assumed to be applicable to both unpyrolyzed cellulose and its activated form. Values of the first two coefficients of the solid molar heat capacity polynomial for the two cellulose compounds are listed in the fourth and fifth columns of the second grouping in Table 2; higher-order coefficients should be set equal to zero.

No heat capacity data could be found in the literature for hemicellulose. However, the heat capacities per unit mass for lignin[10] and cellulose[25] plotted together as functions of temperature (see the Supporting Information) overlap nearly perfectly, suggesting that the same may be true for hemicellulose. As xylan (a biopolymer of xylose) is chemically more like cellulose (a biopolymer of glucose) than lignin (a cross-linked phenolic biopolymer), it is assumed that the mass-based heat capacity of all four hemicelluloses is equivalent to that of cellulose. Values of the first two coefficients of the resulting solid molar heat capacity polynomial for the four hemicellulose compounds are listed in the fourth and fifth columns of the third grouping in Table 2 (higher-order terms should be set equal to zero).

Solid Density Polynomial. Data on the solid density of the holocellulosic and lignin species are scarce. A commonly used assumption is that their densities match that of starch and that they do not vary significantly with temperature.[5] Consequently, the mass density of starch, 1.52 g/cm^3,[14] was used as the basis for the mass density of all 15 solid species and converted to molar densities as shown in the last column in Table 2. These values can be used as the zeroth-order coefficient in a solid density polynomial model, setting all other coefficients equal to zero.

Conventional Fluid Component Parameter Estimates. Among the five conventional fluid compounds, the simplest is 3-hydroxypropanal for which group contribution methods were found to be sufficiently reliable. Triglyceride, the heaviest of the fluid compounds, can be treated as a modified form of linolein which appears in the databanks. *p*-Coumaryl alcohol and sinapyl

DOI: 10.1021/acssuschemeng.9b01278
ACS Sustainable Chem. Eng. 2019, 7, 9017−9027

aldehyde are aromatic products of lignin decomposition that can be treated by a combination of group contribution methods and similarity analysis. Xylosan is chemically similar to levoglucosan, so its properties can also be estimated by a combination of group contribution and similarity analysis methods.

3-Hydroxypropanal. Marrero and Gani's group contribution method[27] can be used to estimate the standard state heat of formation, critical temperature, and critical pressure of 3-hydroxypropanal, while Benson's group contribution method[28−30] can be used for the ideal gas heat capacity. The accuracy of these methods can be readily verified by comparing predicted with accepted values for three similar compounds, *n*-propanal, *n*-propanol, and 4-hydroxybutanal. Details of the estimation calculations as well as a comparison between the accepted values for these compounds and those estimated by these methods are included in the Supporting Information and confirm their efficacy. Values of the ideal gas heat of formation and critical properties as well as the ideal gas heat capacity for 3-hydroxypropanal estimated by these methods are shown in Table 3.

The Aly−Lee equation[31]

$$C_p^{*,ig} = C_{CP,1} + C_{CP,2}\left(\frac{C_{CP,3}/T}{\sinh(C_{CP,3}/T)}\right)^2 + C_{CP,4}\left(\frac{C_{CP,5}/T}{\cosh(C_{CP,5}/T)}\right)^2$$
$$\text{for } C_{CP,6} \le T \le C_{CP,7} \quad (1)$$

was fitted to the estimated ideal gas heat capacities by least-squares regression, resulting in the coefficients shown in the second column of Table 3.

Two measurements of the boiling temperature of 3-hydroxypropanal at reduced pressure can be found in the literature: 38 °C at 0.2 mmHg[32] and 90 °C at 18 mmHg.[33] These provide two vapor pressure data points which can be used in conjunction with Riedel's equation[34] and the previously estimated critical temperature and pressure to fit extended Antoine equation coefficients for 3-hydroxypropanal via the Mani method in Aspen Properties.[35] The form of the Antoine equation used is

$$\ln p^{*,l} = C_{PL,1} + \frac{C_{PL,2}}{T} + C_{PL,3}\ln T + C_{PL,4}T^{C_{PL,5}}$$
$$\text{for } C_{PL,6} \le T \le C_{PL,7} \quad (2)$$

The resulting vapor pressure curve passes close to the data points and terminates at the critical point (see the Supporting Information). The corresponding extended Antoine equation coefficients are listed in Table 3.

With the vapor pressure correlation and critical properties now established, the acentric factor, ω, can be calculated from its definition. The result is $\omega = 1.133$ for 3-hydroxypropanal.

Triglyceride. The molecular formula of triglyceride TGL is given as $C_{57}H_{100}O_7$.[1] However, the number of oxygen atoms in any triglyceride molecule cannot exceed 6, as triglyceride is formed by the triple-condensation reaction of one molecule of glycerol with three molecules of fatty acid. Consequently, the only oxygen-containing functional groups are the three ester groups. To yield a carbon number of 57, each fatty acid should have a carbon number of 18 ($3 \times 18 + 3 = 57$). The fatty acid with carbon number 18 that results in a hydrogen number closest to the given formula is linoleic acid, which has two double bonds. However, the molecular formula of the actual glyceryl trilinoleate, linolein, is $C_{57}H_{98}O_6$. This formula can be matched by adding one oxygen and two hydrogen atoms per molecule of linolein (although that makes it no longer a true triglyceride). The change is minor, given the size of the molecule. Thus, the properties of triglyceride can be approximated by those of linolein, which is used in the production of biodiesel and is included in the databanks. However, some minor adjustments need to be made as indicated below.

In the absence of structural information, there is no basis for estimating vapor pressure and the critical properties from group contribution methods. Therefore, the vapor pressure curve, critical temperature, and critical pressure for triglyceride are assumed to be identical to those for linolein. This means that the acentric factors must also be the same.

The ideal gas enthalpy of formation for triglyceride can be estimated from that of linolein by making corrections for the differences in hydrogen and oxygen number in a manner similar to that used for the lignins. Recalling that the contributions to the molar heat of combustion were found to be −129.1 kJ/g mol/H atom and 208.9 kJ/g mol/O atom, these corrections can also be applied directly to the ideal gas enthalpy of formation

$$\begin{aligned} &{}^{f}\Delta H^{\circ}(\text{triglyceride(g)}) \\ &= {}^{f}\Delta H^{\circ}(\text{linolein(g)}) + 2(-129.1\ \text{kJ/g mol}) + 1(208.9\ \text{kJ/g mol}) \\ &= -1497.0 - 258.2 + 208.9 \\ &= -1546.3\ \text{kJ/g mol} \end{aligned}$$

The ideal gas heat capacity curve can be estimated by adding together the ideal gas molar heat capacities of linolein and water calculated from the correlations in the databanks over a series of intervals along the common temperature range and the Aly and Lee equation[31] fitted to these points by least-squares regression (see the Supporting Information). The fitted parameters are shown in Table 3, together with the other pure component property parameters for triglyceride.

p-Coumaryl Alcohol and Sinapyl Aldehyde. *p*-Coumaryl alcohol and sinapyl aldehyde are aromatic lignin decomposition products with common structural elements. Consequently, the same estimation methods can be used for both compounds.

The Marrero and Gani group contribution method[27] can be used to estimate their critical properties. Critical temperature values estimated by this method for both compounds are shown in Table 3.

Values of certain pure component thermodynamic properties can be estimated from those of similar compounds by calculating the effects of addition or deletion of specific structural elements and adding or subtracting appropriate corrections to account for the differences. For example, *trans*-cinnamic acid, which is included in the databanks is similar to *p*-coumaryl alcohol with two differences: (1) addition of a phenolic hydroxy group in the para position with respect to the acrylic acid group and (2) replacement of the carbonyl oxygen atom in the acrylic acid group with two hydrogen atoms. It is also similar to sinapyl aldehyde with two differences: (1) addition of a phenolic hydroxy group in the para position and methoxy groups in the two meta positions with respect to the acrylic acid group and (2) removal of the hydroxy oxygen in the acrylic acid group.

The ideal gas enthalpy of formation for *trans*-cinnamic acid is in the databanks and agrees with experimental data in the literature[17,36] (see the Supporting Information). Addition of a phenolic hydroxy group in the para position changes *trans*-cinnamic acid to *p*-coumaric acid. This is similar to the addition of a phenolic hydroxy group to toluene to make *p*-cresol. Thus, the ideal gas enthalpy of formation for *p*-coumaric acid can be estimated by adding the difference between the ideal gas

DOI: 10.1021/acssuschemeng.9b01278
ACS Sustainable Chem. Eng. 2019, 7, 9017−9027

enthalpies of formation of *p*-cresol and toluene to the ideal gas enthalpy of formation of *trans*-cinnamic acid from the databanks

$$
\begin{aligned}
{}^{f}\Delta H^{\circ}(p\text{-coumaric acid(g)}) &= {}^{f}\Delta H^{\circ}(\textit{trans}\text{-cinnamic acid(g)}) \\
&+ ({}^{f}\Delta H^{\circ}(\text{cresol(g)}) - {}^{f}\Delta H^{\circ}(\text{toluene(g)})) \\
&= -230.509 + (-125.350 - 50.170) = -406.029\ \text{kJ/g mol}
\end{aligned}
$$

Replacement of the carbonyl oxygen atom in the acrylic acid group with two hydrogen atoms changes *p*-coumaric acid to *p*-coumaryl alcohol. This is analogous to the conversion of acrylic acid to allyl alcohol. Thus, the ideal gas enthalpy of formation for *p*-coumaryl alcohol can be estimated by adding the difference between the ideal gas enthalpies of formation of allyl alcohol and acrylic acid from the databanks to the estimated ideal gas enthalpy of formation of *p*-coumaric acid

$$
\begin{aligned}
{}^{f}\Delta H^{\circ}(p\text{-coumaryl alcohol(g)}) &= {}^{f}\Delta H^{\circ}(p\text{-coumaric acid(g)}) \\
&+ ({}^{f}\Delta H^{\circ}(\text{allyl alcohol(g)}) - {}^{f}\Delta H^{\circ}(\text{acrylic acid(g)})) \\
&= -406.029 + (-124.500 - (-337.060)) = -193.469\ \text{kJ/g mol}
\end{aligned}
$$

so the estimated ideal gas enthalpy of formation for *p*-coumaryl alcohol is −193.5 kJ/g mol. A similar approach can be used to estimate the ideal gas enthalpy of formation for sinapyl aldehyde, −483.8 kJ/g mol (see the Supporting Information). Both values are shown in Table 3.

Vapor pressures of *p*-coumaryl alcohol and sinapyl aldehyde can be estimated from that of *trans*-cinnamic acid (substantiated by experimental data[37]) in an analogous manner. The Supporting Information provides more details. To estimate the vapor pressure of *p*-coumaryl alcohol, the calculated vapor pressure of cinnamic acid at specific temperature intervals was multiplied by the calculated ratio of the vapor pressures of *p*-cresol over toluene (to account for the effect of the addition of the phenolic hydroxy group) and by the calculated ratio of the vapor pressures of allyl alcohol over acrylic acid (to account for the effect of the replacement of the carbonyl oxygen with two hydrogen atoms; vapor pressures at temperatures outside the ranges of individual correlations were extrapolated by maintaining the slope of the natural logarithm of the vapor pressure with respect to inverse temperature). This is equivalent to the following calculation:

$$
\begin{aligned}
\ln p^{*,\mathrm{l}}_{\text{coumaryl-alcohol}}(T) &= \ln p^{*,\mathrm{l}}_{\textit{trans}\text{-cinnamic-acid}}(T) \\
&+ (\ln p^{*,\mathrm{l}}_{p\text{-cresol}}(T) - \ln p^{*,\mathrm{l}}_{\text{toluene}}(T)) \\
&+ (\ln p^{*,\mathrm{l}}_{\text{allyl-alcohol}}(T) - \ln p^{*,\mathrm{l}}_{\text{acrylic-acid}}(T))
\end{aligned}
$$

A similar method was used for sinapyl aldehyde.

Extended Antoine equation coefficients were fitted to the estimated vapor pressure values by nonlinear least-squares regression. The upper limit of the vapor pressure correlation was set at the critical temperature estimated earlier, while the estimated pressure at the critical temperature was used for the critical pressure estimate. The estimates are presented in Table 3.

With the critical properties and vapor pressure correlations available for both compounds, their acentric factors can be calculated from the definition. The result is ω = 1.198 for *p*-coumaryl alcohol and 0.981 for sinapyl aldehyde, as shown in Table 3.

The ideal gas heat capacities of *p*-coumaryl alcohol and sinapyl aldehyde could be estimated from that of *trans*-cinnamic acid in a similar fashion, using correlations with parameters drawn from the databanks. However, the databank parameters for *trans*-cinnamic acid are not based on experimental data but were regressed using values predicted by Benson's method. Consequently, the sensible approach is to use Benson's group contribution method for *p*-coumaryl alcohol and sinapyl aldehyde also. Details are included in the Supporting Information.

Values for the ideal gas heat capacity of *p*-coumaryl alcohol and sinapyl aldehyde estimated using Benson's method are listed in Table 3. The Aly and Lee equation[31] was fitted to these values by least-squares regression, resulting in the parameters for the ideal gas heat capacity correlation for *p*-coumaryl alcohol and sinapyl aldehyde listed immediately below in the same table.

Xylosan. The last compound for which pure component properties are needed is xylosan (1,4-anhydro-α-D-xylopyranose), the dehydration product of the 5-carbon xylose sugar monomer. Its 6-carbon sugar analogue is levoglucosan (1,6-anhydro-β-glucopyranose), which is the dehydration product of the glucose (β-D-glucopyranose) sugar molecule. Levoglucosan is in the databanks, as are glucose and xylose. Consequently, these similarities and relationships can be exploited to estimate the missing properties of xylosan.

Marrero and Gani's method[27] can be used to estimate xylosan's critical properties (see the Supporting Information). The critical temperature value for xylosan estimated in this way is shown in the last column of Table 3.

The ideal gas enthalpy of formation for xylosan can be estimated from the ideal gas enthalpies of formation of levoglucosan, glucose, and xylose if it is assumed that the difference between the values for glucose and levoglucosan is equal to the difference between the values for xylose and xylosan

$$
\begin{aligned}
&{}^{f}\Delta H^{\circ}(\text{glucose(g)}) - {}^{f}\Delta H^{\circ}(\text{levoglucosan(g)}) \\
&\quad = {}^{f}\Delta H^{\circ}(\text{xylose(g)}) - {}^{f}\Delta H^{\circ}(\text{xylosan(g)})
\end{aligned}
$$

This is reasonable, since polycyclic levoglucosan can be formed by removing a water molecule from monocyclic glucose just like polycyclic xylosan can be formed by extracting a water molecule from monocyclic xylose. (Xylose and xylosan have one fewer cyclic −CHOH− than glucose and levoglucosan but are otherwise essentially identical.) The ideal gas enthalpy of formation for levoglucosan in the databanks matches the value recently reported by Rocha et al.[38] (−824.5 kJ/g mol) and can be used for this calculation. Values of the ideal gas enthalpies of formation for glucose and xylose, however, require some substantiation.

Levoglucosan is the dehydration product of β-D-glucopyranose, while the most common naturally occurring glucose stereoisomer and the one for which pure component property data are available is α-D-glucopyranose. The assumption, therefore, will have to be made that thermodynamic properties differences between the α- and β-stereoisomers is negligible.

Ideal gas enthalpies of formation for glucose and xylose in the databanks could not be traced to experimental measurements, so their values were determined using data from the literature. For glucose (α-D-glucopyranose), the value of the solid (crystalline) enthalpy of formation recently reported by Kabo et al.[39] was used in conjunction with the enthalpy of sublimation reported by Oja and Suuberg[40] corrected to 298.15 K using the solid heat capacity at 298.15 K reported by Boerio-Goates[41] and the adjustment proposed by Acree and Chickos.[42] The result is ${}^{f}\Delta H^{\circ}(\text{glucose(g)}) = -1075.9$ kJ/g mol. Similarly, for xylose (α-D-xylopyranose), the solid enthalpy of formation and the solid

DOI: 10.1021/acssuschemeng.9b01278
ACS Sustainable Chem. Eng. 2019, 7, 9017−9027

heat capacity at 298.15 K reported by Ribeiro da Silva et al.[43] together with the enthalpy of sublimation reported by Oja and Suuberg[40] were used with Acree and Chickos'[42] adjustment method to find ${}^{f}\Delta H^{\circ}(\text{xylose(g)}) = -893.7$ kJ/g mol. This allows the ideal gas enthalpy of formation for xylosan to be estimated as

$$\begin{aligned} {}^{f}\Delta H^{\circ}(\text{xylosan(g)}) &= {}^{f}\Delta H^{\circ}(\text{levoglucosan(g)}) + {}^{f}\Delta H^{\circ}(\text{xylose(g)}) \\ &\quad - {}^{f}\Delta H^{\circ}(\text{glucose(g)}) \\ &= -824.5 + (-893.7) - (-1075.9) \\ &= -642.3 \text{ kJ/g mol} \end{aligned}$$

Turning next to the ideal gas heat capacity, although no attribution is provided in the databanks for the source of the parameters for levoglucosan, it can be shown that the correlation matches ideal gas heat capacity values estimated using the Benson method. Consequently, the same approach can be used for xylosan (see the Supporting Information). Fitted parameters for the ideal gas heat capacity correlation for xylosan are listed in the last column of Table 3.

Finally, as was the case for the other pure component parameters, no attribution is provided in the databanks for the source of the vapor pressure correlation values. For levoglucosan, experimental sublimation vapor pressure measurements were reported by Oja and Suuberg[40] and by Kabo et al.[44] Liquid vapor pressure measurements have also been reported,[45] but their accuracy is questionable; they are inconsistent (too high) with the solid vapor pressure data. Solid levoglucosan exhibits a plastic phase transition at 386 K.[40] A (log(pressure) vs inverse temperature) linear fit to Oja and Suuberg's data above 386 K extended to the melting point at 455.4 K coincides with the databank correlation for solid vapor pressure, confirming this as the likely source of the data. The liquid vapor pressure measurements of Epshtein et al.[45] fall well above the extrapolated solid vapor pressure curve, contrary to the expected behavior for the solid−liquid vapor pressure transition, and can be disregarded. The databank liquid vapor pressure correlation is consistent with the solid vapor pressure data, matching the projected sublimation pressure at the melting point and continuing to the critical point (see the Supporting Information). Therefore, the databank vapor pressure correlation for levoglucosan can be used as the starting point for estimating the vapor pressure of xylosan.

Unattributed vapor pressure correlations for glucose and xylose are also available in the databanks, but they are not consistent with sublimation vapor pressure measurements. For example, Oja and Suuberg[40] measured sublimation vapor pressures of glucose over the 395.55−405.78 K temperature range. A (log(pressure) vs inverse temperature) linear fit extrapolated to the reported melting point of 143 °C (416.15 K)[46] yields a vapor pressure of 0.048 Pa. The databank vapor pressure correlation begins at 419.15 K, where it predicts a vapor pressure nearly an order of magnitude higher, 0.433 Pa. Perhaps the databank correlation was influenced by the single vapor pressure measurement at 405.7 K by Kabo et al.,[39] who reported a value of 0.20 Pa, nearly 20 times higher than Oja and Suuberg's measurement of 0.0116 Pa. For the sake of consistency, the vapor pressures of glucose and xylose used to estimate the vapor pressure of xylosan were extrapolated from Oja and Suuberg's sublimation pressure data.

For glucose (α-D-glucopyranose), the value of the enthalpy of fusion at the melting point reported by Roos,[46] 179 J/g at 416.15 K, was corrected to 298.15 K using the solid heat capacity at 298.15 K reported by Boerio-Goates[41] and the adjustment proposed by Acree and Chickos,[42] with the assumption that the solid and liquid heat capacities are identical. The result, 28.2 kJ/g mol, was added to the solid enthalpy of formation to estimate the liquid enthalpy of formation at 298.15 K, −1245.5 kJ/g mol, which, when subtracted from the previously estimated ideal gas enthalpy of formation, results in an estimated enthalpy of vaporization at 298.15 K of 169.6 kJ/g mol. This can now be used to estimate the liquid vapor pressure above the melting point of glucose since the sublimation and liquid vapor pressures are the same at the melting point (0.048 Pa at 416.15 K), and the vapor pressure should initially follow the Clausius−Clapeyron relationship.

For xylose (α-D-xylopyranose), the value of the enthalpy of fusion at the melting point reported by Roos,[46] 211 J/g at 143 °C (416.15 K), was corrected to 298.15 K using the solid heat capacity at 298.15 K reported by Ribeiro da Silva et al.,[43] and the adjustment proposed by Acree and Chickos,[42] with the assumption that the solid and liquid heat capacities are identical. The result, 28.2 kJ/g mol, was added to the solid enthalpy of formation to estimate the liquid enthalpy of formation at 298.15 K, −1026.3 kJ/g mol, which, when subtracted from the previously estimated ideal gas enthalpy of formation, results in an estimated enthalpy of vaporization at 298.15 K of 132.6 kJ/g mol. This can now be used to estimate the liquid vapor pressure above the melting point (416.15 K[46]) of xylose since, as for glucose, the sublimation pressures[40] and liquid vapor pressures are the same at the melting point, and the vapor pressure should initially follow the Clausius−Clapeyron relationship.

With the vapor pressure correlations for levoglucosan, glucose, and xylose thus established, the vapor pressure of xylosan can now be estimated by multiplying the vapor pressure of levoglucosan at any given temperature by the ratio of the vapor pressures of xylose over glucose at that temperature (see the Supporting Information). The lowest temperature included by all three correlations is the melting point of levoglucosan, 455.4 K, while the estimated critical temperature of xylosan is 744.3 K. The pressure calculated at the critical temperature is used as the critical pressure estimate. The extended Antoine equation was fitted to the estimated vapor pressure values of xylosan over this temperature range by least-squares regression, resulting in the fitted parameters listed in the last column of Table 3. The resulting acentric factor of xylosan is 0.292. However, a comparison between the fitted vapor pressure correlation and the vapor pressure calculated by a TV bubble point flash using the PR-BM equation of state shows that the latter predicts 3−8 times higher vapor pressures at temperatures between 283 and 373 K. Increasing the acentric factor to 0.471 allows the PR-BM equation of state to match the correlation in this temperature range (see the Supporting Information).

RESULTS

The effect of the new pure component property parameters on biomass fast pyrolysis simulations was examined. The focus was on assessing the impact of the new thermodynamic properties on the calculated enthalpy changes of individual pyrolysis reactions. Ranzi et al.'s[1] recently published mechanism did not provide estimates of these values for comparison, but some earlier publications did.

Humbird et al.'s[3] entrained-flow, noncatalytic fast pyrolysis process model was used as the test case. This model is based on an earlier multistep kinetic pyrolysis mechanism developed by Ranzi et al. (detailed in the Supporting Information of ref 47) and modified by Trendewicz.[48] The model was independently

DOI: 10.1021/acssuschemeng.9b01278
ACS Sustainable Chem. Eng. 2019, 7, 9017−9027

Table 4. Comparison between Enthalpies of Reaction Used by Humbird et al.[3] and Those Calculated Using the Properties Model

reaction no.	reaction	ΔH_{rxn}(500 °C, 2.3 bar), kJ/kg: Humbird et al.[3]	Aspen Plus energy balance	modified Ranzi et al.[47]
1	CELL → CELLA	0	0	
2	CELLA → 0.8HAA + 0.2GLYOX + 0.1CH3CHO + 0.25HMFU + 0.3ALD3 + 0.21CO2 + 0.1H2 + 0.4CH2O + 0.16CO + 0.83H2O + 0.02HCOOH + 0.61CHAR	620	1139	
3	CELLA → LVG	364	994.7	
4	CELL → 5H2O + 6CHAR	−1913	−1420	
5	HCELL → 0.4HCE1 + 0.6HCE2	100	0	
6	HCE1 → 0.025H2O + 0.775CO2 + 0.025HCOOH + 0.9CO + 0.8CH2O + 0.125C2H5OH + 0.55CH3OH + 0.25C2H4 + 0.525H2 + 0.325CH4 + 0.875CHAR	−92	462.5	358.0
7	HCE1 → 0.25H2O + 0.75CO2 + 0.05HCOOH + 2.15CO + 0.625CH4 + 0.375C2H4 + 1.7H2 + 0.675CHAR	−1860	667.7	544.1
8	HCE1 → XYLAN	588	612.9	
9	HCE2 → 0.2H2O + 1.1CO + 0.675CO2K + 0.5CH2O + 0.1C2H5OH + 0.2HAA + 0.025HCOOH + 0.25CH4 + 0.3CH3OH + 0.275C2H4 + 0.925H2 + CHAR	212	555.2	1395.2
10	LIGC → 0.35LIGCC + 0.1COUMARYL + 0.08PHENOL + 0.41C2H4 + H2O + 0.3CH2O + 1.02CO + 0.7H2 + 0.495CH4 + 5.735CHAR	−490	93.6	61.6
11	LIGH → LIGOH + ALD3	100	237.9	
12	LIGO → LIGOH + CO2	446	0.8	257.0
13	LIGCC → 0.3COUMARYL + 0.2PHENOL + 0.35HAA + 0.7H2O + 1.8CO + 0.65CH4 + 0.6C2H4 + H2 + 6.75CHAR	−503	491.3	198.2
14	LIGOH → LIG + 0.75H2 + 0.9H2O + 0.45CH4 + CH3OH + 0.05CO2 + 1.9CO + 0.05HCOOH + 0.2C2H4 + 4.15CHAR	−120	−90.5	55.7
15	LIGOH → 1.5H2O + 6CO + 1.75CH4 + 4.4H2 + 0.3C2H4 + 0.5CH3OH + 10.15CHAR	−1604	288.4	256.8
16	LIG → FE2MACR	686	967.7	
17	LIG → 0.95H2O + 0.2CH2O + 0.4CH3OH + 1.95CO + 0.6CH4 + 0.05HCOOH + 0.5H2 + 0.65C2H4 + 0.2CH3CHO + 0.2ALD3 + 5.5CHAR	−470	133.3	−102.4
18	LIG → 0.6H2O + 2.6CO + 0.6CH4 + 0.4CH2O + 0.5C2H4 + 0.4CH3OH + 2H2 + 6CHAR	−1663	522.0	238.1
19	H2OL → H2O	2260	642.8	

implemented in aspenONE, and the published results were successfully replicated. However, discrepancies were seen in the reactor energy balance. Specifically, the model implicitly assumes heat losses from the pyrolyzer can be ignored, treating it as an adiabatic process, but when the enthalpies of the feed and product streams were compared, they did not balance. This was found to be due to the use of enthalpies of reaction provided by Ranzi et al.[47] without correcting for the effects of partial volatilization of light products or testing for consistency with the underlying thermodynamic properties model.

Table 4 presents the reaction network used by Humbird et al.[3] The enthalpies of reaction listed in the third last column were used in the energy balance equations in the reactor model, which account for heat transfer from hot sand to the fluidizing gas to the biomass particles, with the reactions either consuming heat from or releasing heat to the biomass, depending on the sign of the enthalpy change (negative exothermic, positive endothermic). Humbird et al. applied these enthalpy changes at reaction conditions with the implicit assumption that they are independent of reaction temperature. The second last column lists the enthalpy change for each reaction as calculated using Aspen Plus and the new properties model at a temperature of 500 °C and pressure of 2.3 bar. A number of discrepancies can be seen.

The enthalpy changes for the first four reactions, which describe cellulose pyrolysis, differ somewhat in magnitude but agree in sign. Reactions 5−9, which describe hemicellulose pyrolysis, however, show significant differences between the values used in the model and those calculated by Aspen Plus. In particular, the pyrolysis of the first activated form of hemicellulose (HCE1, reactions 6 and 7) is exothermic according to the reactor model but endothermic as determined using the Aspen Plus properties model. Interestingly, the values of the enthalpy change for direct decomposition of HCE1 to xylosan (reaction 8) are in near agreement. HCE1 is the predominant activated form obtained from glucomannan softwood hemicellulose according to Ranzi et al.,[1] which would be expected to have a different monomeric formula than xylan hardwood, but the reaction stoichiometry clearly indicates all four hemicellulose species share the xylosan monomer unit basis. (Note that this version of the pyrolysis mechanism does not distinguish between GMSW and XYHW but treats raw hemicellulose as HCELL using the same properties parameters.) More disagreement can be seen for the nine lignin pyrolysis reactions (10−18). Only three are endothermic according to the reactor model (reactions 11, 12, and 16), while only one is exothermic according to the Aspen Plus properties model (reaction 14).

Given the differences between the two reaction enthalpy sets, such that only 2 of the 19 reactions are exothermic according to the properties model compared to 9 exothermic reactions in the reactor model, it should come as no surprise that, for the energy balance around the reactor to close, significantly lower outlet temperatures would be needed than those calculated using the original reaction enthalpies.

The reason for these differences is that the reaction enthalpies used by Humbrid et al.[3] did not match the actual reactions. The original kinetic scheme published by Ranzi et al. featured hemicellulose and lignin decomposition reactions that had partial trapping of volatile species in a metaplastic phase, with defined release kinetics.[47] Humbird et al. assumed instead that all volatile species enter the gas phase immediately.[3] Three of the volatilization "reactions" proposed by Ranzi et al., all involving carbon oxides, are accompanied by substantial changes in enthalpy.[47] Thus, the enthalpy changes of the pyrolysis reactions

DOI: 10.1021/acssuschemeng.9b01278
ACS Sustainable Chem. Eng. 2019, 7, 9017−9027

should have been modified to account for this effect, but they were used instead without change.

The last column in Table 4 shows the corrected enthalpy change for each reaction that involves partial volatilization in the original kinetic scheme. As can be seen there, the differences with the values calculated from the properties model are much smaller. Whereas the arithmetic average difference between the enthalpy changes in the Humbird et al. and properties-based models is greater than 900 kJ/kg, it is only about −14 kJ/kg for the modified Ranzi et al. and properties-based models.

Standard enthalpies of formation for 16 of the 49 species in the properties model were recently reported by Ranzi et al.[1] These values are reproduced in the Supporting Information and compared with the values used in the properties model. With only two exceptions, the enthalpies of formation are not dissimilar. This provides confirmation that the new properties models and parameters give a good representation of the thermodynamics of biomass pyrolysis.

CONCLUSIONS

A properties model for simulating lignocellulosic biomass pyrolysis has been developed, incorporating model compounds not found in commercial process simulator databanks. The objective was to enable process simulations based on a recently published lumped kinetics model.[1] Standard solid enthalpy of formation, solid heat capacity, and solid density estimates based on the limited experimental data available were prepared for 15 biomass constituents and intermediate and end-products of their pyrolysis. Ideal gas enthalpy of formation and heat capacity, critical property, and vapor pressure estimates were prepared for another five compounds. Addition of these new components and properties allows thermodynamically rigorous simulation of lumped biomass pyrolysis reactions with accurate energy balances. Enthalpies of reaction calculated from the properties model were compared with reported reaction enthalpies for the same lumped biomass pyrolysis reactions and found to be in general agreement.

This properties model can be used in simulations of different biomass pyrolysis processes using the same model compounds. The pyrolysis mechanism and components, while widely used, may not be appropriate for all pyrolysis models. However, the component list can be easily extended by adding missing components. Furthermore, the property parameter estimation methodology can be used for any new compounds that may arise as the biomass pyrolysis process model development project evolves.

ASSOCIATED CONTENT

Supporting Information

The Supporting Information is available free of charge on the ACS Publications website at DOI: 10.1021/acssuschemeng.9b01278.

Additional supporting calculations (PDF)

AUTHOR INFORMATION

Corresponding Author

*Phone: +1 803 725-1314. E-mail: maximilian.gorensek@srnl.doe.gov.

ORCID

Maximilian B. Gorensek: 0000-0002-4322-9062

Chau-Chyun Chen: 0000-0003-0026-9176

Author Contributions

The manuscript was written through contributions of all authors. All authors have given approval to the final version of the manuscript. All authors contributed equally.

Funding

Funding support was provided by the US Department of Energy under grant DE-EE0007888-02-7. C.-C.C. and R.S. gratefully acknowledge the financial support of the Jack Maddox Distinguished Engineering Chair Professorship in Sustainable Energy, sponsored by the J.F Maddox Foundation. SRNL is operated for the DOE's Office of Environmental Management (DOE-EM) by Savannah River Nuclear Solutions, LLC, under Contract DE-A C09-08SR22470.

Notes

The authors declare no competing financial interest.

ACKNOWLEDGMENTS

This report was prepared as an account of work sponsored by an agency of the United States Government. Neither the United States Government nor any agency thereof, nor any of their employees, makes any warranty, express or implied, or assumes any legal liability or responsibility for the accuracy, completeness, or usefulness of any information, apparatus, product, or process disclosed, or represents that its use would not infringe privately owned rights. Reference herein to any specific commercial product, process, or service by trade name, trademark, manufacturer, or otherwise does not necessarily constitute or imply its endorsement, recommendation, or favoring by the United States Government or any agency thereof. The views and opinions of authors expressed herein do not necessarily state or reflect those of the United States Government or any agency thereof.

REFERENCES

(1) Ranzi, E.; Debiagi, P. E. A.; Frassoldati, A. Mathematical Modeling of Fast Biomass Pyrolysis and Bio-Oil Formation. Note I: Kinetic Mechanism of Biomass Pyrolysis. *ACS Sustainable Chem. Eng.* **2017**, *5* (4), 2867−2881.

(2) Dutta, A.; Sahir, A.; Tan, E.; Humbird, D.; Snowden-Swan, L. J.; Meyer, P.; Ross, J.; Sexton, D.; Yap, R.; Lukas, J. L. *Process Design and Economics for the Conversion of Lignocellulosic Biomass to Hydrocarbon Fuels. Thermochemical Research Pathways with In Situ and Ex Situ Upgrading of Fast Pyrolysis Vapors*; Technical Report NREL/TP-5100-62455 for National Renewable Energy Laboratory: Golden, CO, March 1, 2015. DOI: 10.2172/1215007.

(3) Humbird, D.; Trendewicz, A.; Braun, R.; Dutta, A. One-Dimensional Biomass Fast Pyrolysis Model with Reaction Kinetics Integrated in an Aspen Plus Biorefinery Process Model. *ACS Sustainable Chem. Eng.* **2017**, *5* (3), 2463−2470.

(4) Peters, J. F.; Banks, S. W.; Bridgwater, A. V.; Dufour, J. A kinetic reaction model for biomass pyrolysis processes in Aspen Plus. *Appl. Energy* **2017**, *188*, 595−603.

(5) Wooley, R. J.; Putsche, V. *Development of an ASPEN PLUS Physical Property Database for Biofuels Components*; Technical Report NREL/TP-425-20685 for National Renewable Energy Laboratory: Golden, CO, April 1996.

(6) Jones, S.; Meyer, P.; Snowden-Swan, L.; Padmaperuma, A.; Tan, E.; Dutta, A.; Jacobson, J.; Cafferty, K. *Process Design and Economics for the Conversion of Lignocellulosic Biomass to Hydrocarbon Fuels: Fast Pyrolysis and Hydrotreating Bio-oil Pathway*; Technical Report NREL/TP-5100-61178 for National Renewable Energy Laboratory: Golden, CO, November 1, 2013. DOI: 10.2172/1126275.

(7) Boston, J. F.; Mathias, P. M. In *Phase Equilibria in a Third-Generation Process Simulator*, Proceedings of the 2nd International

DOI: 10.1021/acssuschemeng.9b01278
ACS Sustainable Chem. Eng. 2019, 7, 9017−9027

Conference on Phase Equilibria and Fluid Properties in the Chemical Process Industries,, West Berlin, March 17−21, 1980; pp 823−49.
(8) *Aspen Plus*, V10.0; Aspen Technology, Inc.: Burlington, MA, 2017.
(9) Greenstein, J. P.; Winitz, M. *Chemistry of the amino acids*; Robert E. Kreiger Publishing Co.: Malabar, FL, 1984; Vol. *1*.
(10) Voitkevich, O. V.; Kabo, G. J.; Blokhin, A. V.; Paulechka, Y. U.; Shishonok, M. V. Thermodynamic Properties of Plant Biomass Components. Heat Capacity, Combustion Energy, and Gasification Equilibria of Lignin. *J. Chem. Eng. Data* **2012**, *57* (7), 1903−1909.
(11) Maksimuk, Y.; Ponomarev, D.; Sushkova, A.; Krouk, V.; Vasarenko, I.; Antonava, Z. Standard molar enthalpy of formation of vanillin. *J. Therm. Anal. Calorim.* **2018**, *131* (2), 1721−1733.
(12) Maksimuk, Y.; Antonava, Z.; Ponomarev, D.; Sushkova, A. Standard molar enthalpies of formation for crystalline vanillic acid, methyl vanillate and acetovanillone by bomb calorimetry method. *J. Therm. Anal. Calorim.* **2018**, *134* (3), 2127−2136.
(13) Gundry, H. A.; Harrop, D.; Head, A. J.; Lewis, G. B. Thermodynamic properties of organic oxygen compounds 21. Enthalpies of combustion of benzoic acid, pentan-1-ol, octan-1-ol, and hexadecan-1-ol. *J. Chem. Thermodyn.* **1969**, *1* (3), 321−332.
(14) Rumble, J. R., Ed. *CRC Handbook of Chemistry and Physics*, 99th ed. (Internet Version 2018); CRC Press/Taylor & Francis: Boca Raton, FL, 2019.
(15) Monte, M. J. S.; Gonçalves, M. V.; Ribeiro da Silva, M. D. M. C. Vapor Pressures and Enthalpies of Combustion of the Dihydroxybenzoic Acid Isomers. *J. Chem. Eng. Data* **2010**, *55* (6), 2246−2251.
(16) Ribeiro da Silva, M. A. V.; Ferreira, A. I. M. C. L.; Lima, L. s. M. S. S.; Sousa, S. M. M. Thermochemistry of phenylacetic and monochlorophenylacetic acids. *J. Chem. Thermodyn.* **2008**, *40* (2), 137−145.
(17) Parks, G. S.; Mosher, H. P. Heats of Combustion and Formation of Seven Organic Compounds Containing Oxygen. *J. Chem. Phys.* **1962**, *37* (4), 919−920.
(18) Kirklin, D. R. Enthalpy of combustion of acetylsalicylic acid. *J. Chem. Thermodyn.* **2000**, *32* (6), 701−709.
(19) Speros, D. M.; Rossini, F. D. Heats of Combustion and Formation of Naphthalene, the Two Methylnaphthalenes, cis and trans-Decahydronaphthalene, and Related Compounds. *J. Phys. Chem.* **1960**, *64* (11), 1723−1727.
(20) Nagano, Y. High-precision micro-combustion calorimetry of anthracene. *J. Chem. Thermodyn.* **2001**, *33* (4), 377−387.
(21) Smith, N. K.; Stewart, R. C.; Osborn, A. G.; Scott, D. W. Pyrene: vapor pressure, enthalpy of combustion, and chemical thermodynamic properties. *J. Chem. Thermodyn.* **1980**, *12* (10), 919−926.
(22) Wagman, D. D.; Evans, W. H.; Parker, V. B.; Schumm, R. H.; Halow, I.; Bailey, S. M.; Churney, K. L.; Nuttall, R. L. The NBS tables of chemical thermodynamic properties; Selected values for inorganic and C_1 and C_2 organic substances in SI units. *J. Phys. Chem. Ref. Data* **1989**, *18* (4), 1807.
(23) Yin, C.-Y. Prediction of higher heating values of biomass from proximate and ultimate analyses. *Fuel* **2011**, *90* (3), 1128−1132.
(24) Channiwala, S. A.; Parikh, P. P. A unified correlation for estimating HHV of solid, liquid and gaseous fuels. *Fuel* **2002**, *81* (8), 1051−1063.
(25) Blokhin, A. V.; Voitkevich, O. V.; Kabo, G. J.; Paulechka, Y. U.; Shishonok, M. V.; Kabo, A. G.; Simirsky, V. V. Thermodynamic Properties of Plant Biomass Components. Heat Capacity, Combustion Energy, and Gasification Equilibria of Cellulose. *J. Chem. Eng. Data* **2011**, *56* (9), 3523−3531.
(26) Ioelovich, M. Y. Comparison of methods for the calculation of heat of combustion of biopolymers. *Khim. Rastit. Syr'ya* **2017**, No. 2, 49−56.
(27) Marrero, J.; Gani, R. Group-contribution based estimation of pure component properties. *Fluid Phase Equilib.* **2001**, *183−184*, 183−208.
(28) Benson, S. W.; Buss, J. H. Additivity Rules for the Estimation of Molecular Properties. Thermodynamic Properties. *J. Chem. Phys.* **1958**, *29* (3), 546−572.
(29) Benson, S. W.; Cruickshank, F. R.; Golden, D. M.; Haugen, G. R.; O'Neal, H. E.; Rodgers, A. S.; Shaw, R.; Walsh, R. Additivity rules for the estimation of thermochemical properties. *Chem. Rev.* **1969**, *69* (3), 279−324.
(30) Poling, B. E.; Prausnitz, J. M.; O'Connell, J. P. *The Properties of Gases and Liquids*, 5th ed.; McGraw-Hill Education: New York, 2000.
(31) Aly, F. A.; Lee, L. L. Self-consistent equations for calculating the ideal gas heat capacity, enthalpy, and entropy. *Fluid Phase Equilib.* **1981**, *6* (3), 169−179.
(32) Hall, R. H.; Stern, E. S. 96. Acid-catalysed hydration of acraldehyde. Kinetics of the reaction and isolation of *β*-hydroxypropaldehyde. *J. Chem. Soc.* **1950**, *0* (0), 490−498.
(33) Stepanova, A. V.; Shchukinoi, M. To the question of the aldol condensation of formaldehyde and acetaldehyde. *Zhurnal Russkogo fiziko-khimicheskogo obshchestva (Journal of the Russian Physico-Chemical Society)* **1926**, *58* (7), 840−848.
(34) Riedel, L. Eine neue universelle Dampfdruckformel Untersuchungen über eine Erweiterung des Theorems der übereinstimmenden Zustände. Teil I. *Chem. Ing. Tech.* **1954**, *26* (2), 83−89.
(35) *Aspen Properties*, V10.0; Aspen Technology, Inc.: Burlington, MA, 2017.
(36) Monte, M. J. S.; Hillesheim, D. M. Vapour pressures, enthalpies and entropies of sublimation of trans -cinnamic acid and of nine methoxy and dimethoxycinnamic acids. *J. Chem. Thermodyn.* **1999**, *31* (11), 1443−1456.
(37) Stull, D. R. Vapor Pressure of Pure Substances. Organic and Inorganic Compounds. *Ind. Eng. Chem.* **1947**, *39* (4), 517−540.
(38) Rocha, I. M.; Galvão, T. L. P.; Sapei, E.; Ribeiro da Silva, M. D. M. C.; Ribeiro da Silva, M. A. V. Levoglucosan: A Calorimetric, Thermodynamic, Spectroscopic, and Computational Investigation. *J. Chem. Eng. Data* **2013**, *58* (6), 1813−1821.
(39) Kabo, G. J.; Voitkevich, O. V.; Blokhin, A. V.; Kohut, S. V.; Stepurko, E. N.; Paulechka, Y. U. Thermodynamic properties of starch and glucose. *J. Chem. Thermodyn.* **2013**, *59*, 87−93.
(40) Oja, V.; Suuberg, E. M. Vapor Pressures and Enthalpies of Sublimation of d-Glucose, d-Xylose, Cellobiose, and Levoglucosan. *J. Chem. Eng. Data* **1999**, *44* (1), 26−29.
(41) Boerio-Goates, J. Heat-capacity measurements and thermodynamic functions of crystalline *α*-D-glucose at temperatures from 10 to 340 K. *J. Chem. Thermodyn.* **1991**, *23* (5), 403−409.
(42) Acree, W., Jr.; Chickos, J. S. Phase Transition Enthalpy Measurements of Organic and Organometallic Compounds. Sublimation, Vaporization and Fusion Enthalpies From 1880 to 2010. *J. Phys. Chem. Ref. Data* **2010**, *39* (4), 043101.
(43) Ribeiro da Silva, M. A. V.; Ribeiro da Silva, M. D. M. C.; Lobo Ferreira, A. I. M. C.; Shi, Q.; Woodfield, B. F.; Goldberg, R. N. Thermochemistry of *α*-D-xylose(cr). *J. Chem. Thermodyn.* **2013**, *58*, 20−28.
(44) Kabo, G. J.; Paulechka, Y. U.; Voitkevich, O. V.; Blokhin, A. V.; Stepurko, E. N.; Kohut, S. V.; Voznyi, Y. V. Experimental and theoretical study of thermodynamic properties of levoglucosan. *J. Chem. Thermodyn.* **2015**, *85*, 101−110.
(45) Epshtein, Y. V.; Durynina, L. I.; Pashinkin, A. S. The vapor pressure of levoglucosan (*β*-1,6-anhydroglucopyranose) (transl.). *Zhurnal prikladnoi khimii/Russkoe fiziko-khimicheskoe obshchestvo* **1964**, *37* (11), 2543−2545.
(46) Roos, Y. Melting and glass transitions of low molecular weight carbohydrates. *Carbohydr. Res.* **1993**, *238*, 39−48.
(47) Ranzi, E.; Corbetta, M.; Manenti, F.; Pierucci, S. Kinetic modeling of the thermal degradation and combustion of biomass. *Chem. Eng. Sci.* **2014**, *110*, 2−12.
(48) Trendewicz, A. A. *Development of a circulating fluidized bed reactor model for the fast pyrolysis of biomass for process simulation*. Thesis, Colorado School of Mines, Golden, CO, 2015.

DOI: 10.1021/acssuschemeng.9b01278
ACS Sustainable Chem. Eng. 2019, 7, 9017−9027